Lamellar Diblock Copolymer Grain Boundary Morphology. 1. Twist Boundary Characterization

Samuel P. Gido,† Janelle Gunther, and Edwin L. Thomas*

Department of Materials Science and Engineering, Program in Polymer Science and Technology, Massachusetts Institute of Technology, Cambridge, Massachusetts 02139

David Hoffman

Department of Mathematics and Statistics, University of Massachusetts, Amherst, Massachusetts 01003

Received December 22, 1992; Revised Manuscript Received May 6, 1993

ABSTRACT: Grain boundary morphologies in poly(styrene-*b*-butadiene) lamellar diblock copolymers were characterized using transmission electron microscopy (TEM). Two types of twist grain boundaries were observed in which microphase separation of the two blocks was maintained in the grain boundary region by intermaterial dividing surfaces that approximate classically known minimal surfaces. The geometry of these interfaces was demonstrated by comparing experimental TEM images with ray tracing computer simulations of the model surfaces as the projection direction was systematically varied in both the experimental and simulated images. The two morphologies observed were found to have intermaterial dividing surfaces that approximate either Scherk's first (doubly periodic) surface or a section of the right helicoid. The helicoid section boundary was observed at low twist angles, less than or equal to about 15°. The Scherk surface family of boundary morphologies, which consists of a doubly periodic array of saddle surfaces, was found over the entire twist range from 0 to 90°. As the twist angle approaches 0° the Scherk surface grain boundary morphology is transformed into a single screw dislocation that has an intermaterial dividing surface with the geometry of a single helicoid. Direct TEM imaging of the detailed core structure of this screw dislocation is presented. These images demonstrate that in the lamellar diblock copolymer the screw dislocation core is nonsingular. This nonsingular core structure represents a radical departure from the sigular core structures observed in classical studies of dislocations in atomic crystals.

I. Introduction

Diblock copolymer materials that form microphase separated morphologies such as spheres, cylinders, ordered bicontinuous double diamond (OBDD), and lamella also form larger scale grain structures. Figure 1 shows a transmission electron microscope (TEM) image of a thin section of such a lamellar grain structure in a diblock copolymer. The inset is a schematic representation of the three dimensional, lamellar grain structure. The micrograph is a projected image of a thin slice taken from this type of structure. The specific structure of the boundary regions between grains has a great impact on material properties, such as elastic modulus and gas permeability, that depend on the continuity of the individual phases across the grain boundaries. In fact, experimental investigations of macroscopic transport and mechanical properties of styrene–isoprene (SI) and styrene–butadiene (SB) block copolymers strongly suggest that phase continuity is generally maintained across these boundaries.[1,2] This paper is the first in a series of four that presents characterization and modeling of grain boundary morphologies in compositionally symmetric diblock copolymers forming lamellar morphologies. Throughout this paper we will refer to the following three papers of the series as GB-II,[3] GB-III,[4] and GB-IV.[5]

Although grain structure and grain boundary morphology are critical aspects of structure–property relationships, experimental and theoretical work to date has generally concentrated on the basic equilibrium microdomain morphologies (spheres, cylinders, OBDD, and lamella). Grain boundaries and other defects are nonequilibrium, metastable structures. Previous work has been concerned with establishing the scaling relationships between domain spacing and molecular weight in the equilibrium morphologies[6-10] and on theoretically predicting[6-8,11] and experimentally verifying[12] morphology vs composition diagrams and the order–disorder transition.[11,13-15] Bates and Fredrickson have recently reviewed both experimental and theoretical aspects of previous work on the equilibrium morphologies of diblock copolymers.[16]

Before proceeding to discuss grain boundary morphology, it is necessary to briefly describe an approach to modeling block copolymer morphologies based on geometrical surfaces of constant mean curvature. We begin by discussing the equilibrium diblock morphologies, and then we will extend this approach to nonequilibrium defect structures such as grain boundaries. In the strong segregation regime, the microphase separated diblock domains—polystyrene (PS) and polybutadiene (PB) domains for instance—are separated by an interfacial region which we will call the intermaterial dividing surface (IMDS). The observed, equilibrium IMDS's are the result of factors that lead to strongly segregated microphases in amorphous diblock copolymers:[6-8,14,17-22] The van der Waals interaction between unlike monomer units in the PS and PB blocks is unfavorable with respect to the interaction between like monomer units. The resulting microphase separation leads to strongly segregated microphases separated by a narrow IMDS. The IMDS's have an associated energy per unit area or interfacial tension and thus tend to minimize their surface areas. However, the polymer within the microdomains is essentially incompressible, and the diblock chains are entropy springs that resist deformation into highly extended or compressed conformations. These physical factors place a limit on the amount that the IMDS can reduce its surface area.

The IMDS is actually a region about 20 Å thick[9,10,21,23,24] that contains the covalent junctions between the unlike

* To whom correspondence should be addressed.
† Present address: Department of Polymer Science and Engineering, University of Massachusetts, Amherst, MA 01003.

0024-9297/93/2226-4506$04.00/0

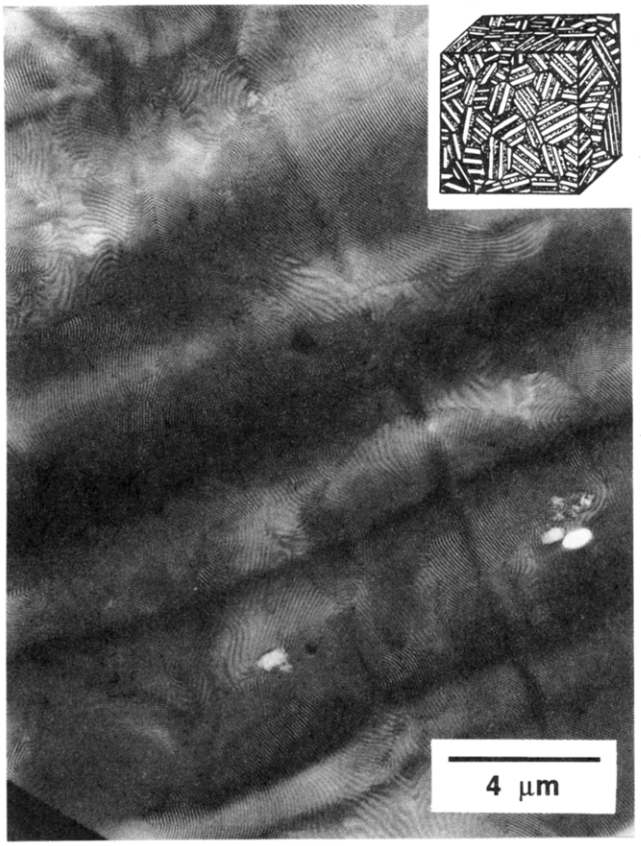

Figure 1. TEM micrograph showing the grain structure in a lamella forming poly(styrene-*b*-butadiene) diblock copolymer: PS 81 000; PB 74 400 (designated SB 80/80). The inset shows a schematic illustration of the three dimensional grain structure. [Inset reproduced with modifications from: Sax, J. E.; Ottino, J. M. *Polym. Eng. Sci.* **1983**, *23*, 165.]

blocks (as well as many nonbonded PS–PB interactions) and separates the two microphases. Compared to the microdomain thickness of about 100–300 Å, depending on molecular weight, the interfacial region is quite thin and thus will be modeled as a 2D surface.

On the basis of the analysis of TEM micrographs and on the preceding free energy considerations, minimal surfaces and surfaces of constant mean curvature (CMC) have been proposed as approximate models for the IMDS's of block copolymer microdomain morphologies.[22,25,26] Mean curvature (H) is defined pointwise on a surface to be the average of the two principal curvatures (reciprocals of the principal radii of curvature). If the mean curvature is constant on a surface, then the surface is a *local* solution for the following variational problem: Minimize surface area subject to a volume contraint. In the application to block copolymers, this volume constraint is given by the volume fractions of the two microphases. The IMDS's in the spherical, cylindrical, OBDD, and lamellar equilibrium morphologies are all CMC surfaces. It should be emphasized, however, that the condition of constant mean curvature is determined locally and does not imply that all these surfaces are necessarily global minima for area with respect to the fixed volume constraint. Global interfacial area (interfacial energy) minimization would require coalescence of the dispersed phase into ever larger spherical regions which eventually lead to a single flat interface separating two macroscopic phases. This is indeed the type of behavior observed with two immiscible fluids such as oil and water or a blend of two homopolymers. Periodic arrangements of small spheres, cylinders, OBDD, and lamella, while all of CMC, only represent local interfacial area minima. The reason that these periodic, small-scale morphologies are observed in block copolymers is that they minimize the local interfacial area of small domains composed of block copolymers that are constrained to have their junction points on the IMDS. These domains must be small enough to allow the respective block chains to stretch in and uniformly fill their interiors.

A surface whose mean curvature is identically zero is called a minimal surface.[22,26–33] Minimal surfaces form a subset of the CMC surfaces. Mathematically, minimal surfaces result when the volume fraction constraints on the area minimization are 50/50 or, alternatively, when these volume constraints are completely removed. In the block copolymer physical analog, the lamellar morphology has minimal surface interfaces, since both the principal curvatures are zero everywhere on a plane. Here the volume fractions must be nearly, but need not be exactly, 50/50. Minimal surfaces are not always flat however. As long as a surface curves equally in two opposite directions at each point it can maintain zero mean curvature. There are in fact many examples of curved minimal surfaces, for instance the lamellar catenoid structure.[22,34,35] Other minimal surfaces have been proposed as models for interfaces in microemulsions,[28,30,32,33] as equipotential surfaces in electrically conductive solids,[32] and as models for zeolite structures.[31]

Having discussed the general geometric properties of IMDS's in the equilibrium diblock morphologies, we now extend these principles to grain boundary morphologies in lamellar diblocks. In strongly segregated and annealed specimens, the planar intermaterial dividing surfaces (IMDS) separating the lamellar microdomains are approximately parallel to one another within each grain. There is some cooperative, gentle bending and undulation of these IMDS's, but we will consider such gentle changes of lamellar orientation over relatively long distances as distinct from grain boundaries which are defined as localized, abrupt changes in the orientation of many lamella. TEM micrographs of block copolymers in the literature[2,36,37] contain numerous examples of such localized grain boundaries. However, such micrographs were generally used to illustrate some other morphological point, and the grain boundaries themselves have not been systematically investigated.

Grain boundaries in three dimensional crystalline materials, such as metals and ceramics, have five degrees of twist–tilt freedom,[38,39] of which only two are important for describing grain boundaries in lamellar block copolymers, a system with only one dimensional symmetry. These two degrees of freedom, shown in Figure 2, are tilt and twist. The angle θ gives the tilt relationship between two lattices. This tilt angle is measured about an axis parallel to the grain boundary. In a general crystalline material, with a 3D lattice, tilt is resolved into two angles, θ_1 and θ_2, which occur about two orthogonal axes. In the case of lamellar materials only one tilt angle (measured in a plane orthogonal to the lamella) is present. Tilt is discussed in greater detail in GB-IV. The present paper concentrates on twist boundaries which, as shown in Figure 2c, are characterized by the angle, α. This twist angle is measured about an axis perpendicular to the grain boundary.

The twist and tilt degrees of freedom specify general constraints on the material in the grain boundary region. Grain boundary morphologies must minimize energy within the geometrical constraints imposed by the adjoining, misaligned, bulk grains. The diblock material remains microphase separated within the grain boundary region but must merge continuously into the adjoining equilibrium grain structures. The interface between the two types of domains in the grain boundary region

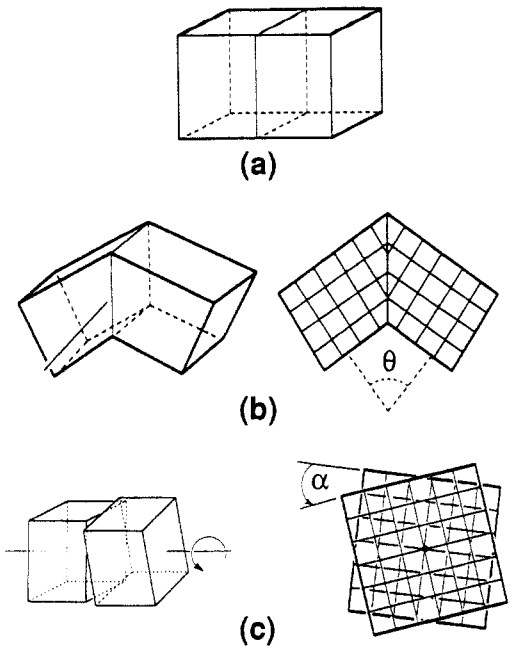

Figure 2. Grain boundary geometry. (a) The reference state is an aligned bicrystal with no boundary. (b) A tilt boundary is produced by rotating the grains with respect to one another about an axis which, as shown, is parallel to the plane of the grain boundary. The angle θ gives the tilt relationship between lattices on the opposite side of the boundary. (c) A twist boundary is produced by rotating the grains with respect to one another about an axis which, as shown, is perpendicular to the plane of the grain boundary. The angle α measures the twist of the lattice across the grain boundary.

separates these two microphases while minimizing the sum of interfacial and chain stretching energies as much as possible subject to the geometrical constraints of the boundary. Thus grain boundary morphologies are local, equilibrium structures. The interfacial surface between the microdomains in the grain boundary region thus has many of the characteristics of the IMDS previously defined for the equilibrium diblock morphologies. However, it represents a local rather than a global equilibrium. Thus we will continue to recognize the distinction between the equilibrium IMDS's within the grains and the interfacial structure in the grain boundary region, which we will call IMDS†. The constrained, local equilibrium structures of other types of defects such as disclinations and dislocations are likewise designated IMDS†. The IMDS† describing a grain boundary region must merge continuously with the respective microdomain IMDS's at the edges of the boundary region.

It is known that the average grain size increases as diblock copolymer materials are annealed at elevated temperatures. An increase in grain size with annealing is also observed, and well understood,[40] in metals. The grain boundaries as defect structures possess higher energy than the material within the grains. In 3D crystalline materials, and presumably in the diblock copolymer case as well, grain growth is driven by the corresponding decrease in the total amount of grain boundary area separating the grains as they grow larger. The twist grain boundary morphologies that will be presented in this paper have structures that are conducive to easy grain boundary motion. Our present experimental methods do not, however, allow us to directly observe grain boundary motion. In subsequent papers, grain boundary energies will be calculated which provide a measure of the amount by which the total energy of the diblock material can be reduced through grain growth.

Minimal and CMC surfaces are solutions to mathematical problems involving only area minimization (surface energy). The contribution of chain conformational energies in the free energy functional to be minimized dictate that in many cases the physical solutions cannot be exactly minimal or CMC surfaces. However, the deviation of the block copolymer grain boundary interfaces observed in previous morphological investigations,[22,25] and in this study, from the minimal and CMC surface models is so slight as to be undetectable with current experimental techniques.

Diblock copolymers may be likened to macromolecular analogs of smectic A liquid-crystalline materials. Theoretically, for small molecule smectic A materials, in the absence of strong external fields, surface defects (twist walls or tilt walls) are unstable and should break up into separate line defects such as edge dislocations[41,42] or focal conic arrangements of disclinations. Surface defects may also be expected to delocalize into long range bends or twists of the smectic layers (lamella). Common smectic A liquid crystals thus do not exhibit grain structures but instead delocalize distortions as much as possible. In the block copolymer case studied here, there is an observed prevalence of localized surface (planar) defects, which we will call grain boundaries. The tendency of these grain boundaries to remain localized, which is experimentally verfied by the TEM micrographs presented in this paper, is addressed in the content of the grain boundary energy calculations in subsequent papers.

In block copolymer samples, in which the microstructure has been allowed to equilbrate (slow, static film casting from solution followed by long term annealing at elevated temperature), localized surface defects (i.e. grain boundaries) are commonly observed. Close examination of Figure 1 reveals, in addition to grain boundaries, numerous disclinations of strength $\pm^1/_2$ as well as edge dislocations. There are some regions in which the lamella undergo long range, gentle bending around disclination cores as in a focal conic texture. However, there is an overwhelming prevalence for localized surface defects, which gives the block copolymer microstructure an appearance more similar to the familiar grain structures of metals or ceramics. A recent theoretical paper by Fredrickson and Binder[13] (discussed in GB-II) indicates how lamellar block copolymer morphologies might form by a first order nucleation and growth mechanism, thus explaining the grain-like block copolymer morphologies that we observe. Grain boundaries form when growing grains of different orientations impinge upon one another. The IMDS†'s that form between the microphases in the region of impingement determine the grain boundary morphology.

This paper will concentrate on the structural characterization of twist grain boundaries in lamellar block copolymers. The lamellar diblock twist boundary morphologies share some structural characteristics of the A* or twist grain boundary (TGB) phase recently reported in small molecule smectic liquid crystals.[43-45] In the TGB phase the grain boundaries occur with a regular periodicity and are an integral part of the equilibrium phase. The grain boundary structures we observe in diblock copolymers are metastable defects, not a thermodynamic phase, and they occur with a random distribution throughout the material. However, the geometric requirements of joining lamellar layers across a concentrated region of twist reorientation are shared by both the diblock twist boundaries and the TGB phase. Recent TEM characterization of the TGB phase required the use of freeze-fracture surface replicas.[46,47] Although the periodically spaced grain boundary regions were clearly observable, very little detail of the structure within these boundary regions was detectable. Direct TEM observation of the details of the material geometry in the grain boundary region is, however,

possible with the SB diblock copolymers used in this study. The detailed characterization of twist boundary geometry reported in this paper may have applicability to the structure of grain boundaries in the TGB phase.

Direct imaging of grain boundaries through TEM, coupled with theoretical modeling, is used to develop a unified approach for understanding the structure of grain boundaries in lamellar diblock materials. In this paper, two families of pure twist grain boundary morphologies are characterized by TEM and minimal surface IMDS† models for these structures are proposed. GB-II and -III present grain boundary energy calculations for the two twist boundary morphological families which were discovered in this study. In GB-IV pure tilt boundary morphologies are characterized with TEM. The understanding of lamellar diblock copolymer grain boundary morphology presented in these four papers may provide the starting point for modeling the effects of grain boundary structure and phase continuity on polymer material properties.

II. Experimental Section

The materials examined are lamellar forming, nearly symmetric diblock copolymers with molecular weights[48] 20 500/20 500, 42 300/45 400, and 81 000/74 400 (designated SB 20/20, 40/40, and 80/80). The PS volume fractions for SB 20/20, 40/40, and 80/80 are 0.456, 0.438, and 0.477, respectively.

These materials are highly monodisperse ($M_w/M_n \leq 1.05$), anionically synthesized copolymers made by Dr. L. J. Fetters of Exxon. Samples were static cast from a 10 weight % solution in toluene over a period of 1 week. The resulting ~1-mm-thick films were annealed under vacuum at 115 °C for another week, after which they were quenched in liquid nitrogen and then allowed to warm to room temperature. Thus the morphology observed is characteristic of the material at 115 °C.

The block copolymer bulk films were then prepared for TEM observation. Approximately 700-Å-thick sections were cut by cryoultramicrotomy using a diamond knife at −100 °C. These sections were collected on copper TEM grids and stained in OsO_4 vapor for 4 h. The stain reacts preferentially with the double bonds in the butadiene blocks, rendering the PB microdomains dark via mass–thickness contrast in TEM micrographs. The samples were then observed in a JEOL 200CX TEM operated at 200 kV, employing either a tungsten or a LaB_6 filament. Single tilt and double tilt goniometer stages were used.

In order to compare TEM images of grain boundary morphologies with geometric models, computer ray tracing was utilized to produce simulated micrographs based on these models for comparison with the experimental data. These simulations were produced using a software package called *Polyworks*.[49] A three dimensional matrix containing up to 100 million simulated volume elements was created in the memory of a Cray XMP supercomputer. This simulated material volume was divided into layers representing two lamellar phases of the diblock and including a grain boundary region of the model geometry to be simulated. Each volume element was given a numerical value, 0 or 1, to identify it as belonging to one of the two diblock phases. This simulated region of material around the grain boundary was truncated by parallel horizontal planes in order to mimic microtoming. Then lines or rays are passed through the simulated sample and projected onto a plane to form an image based on the relative amounts of light and dark material that each ray has encountered. It is possible to change the orientation of the simulated sample with respect to the image forming rays in order to simulate tilting the diblock specimen in the TEM. This utility allowed simulation of TEM series in which micrographs of the same feature were taken at a number of systematically varied sample tilts. Such a tilt series is generally required in order to identify a complex three dimensional morphology from two dimensional projected images.

The determination of the three dimensional geometry of a grain boundary from projected TEM images requires an independent knowledge of the specimen thickness and the lamellar long period. It involves information taken from the micrograph such as the change in projected lamellar fringe spacing across the boundary, from which the magnitude of the twist angle is determined.

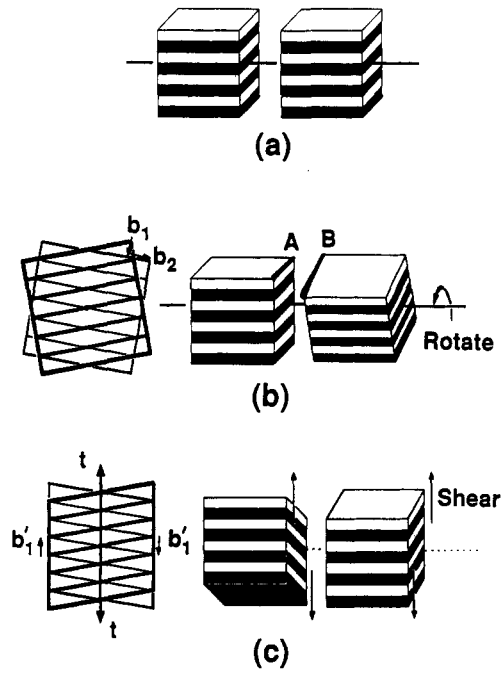

Figure 3. Hypothetical process to create a low angle twist boundary. (a) The reference state is an aligned bicrystal with no boundary. (b) A twist grain boundary is produced by rotation of one grain with respect to the other about an axis passing through the centers of both grains. This boundary contains an array of two orthogonal sets of screw dislocations with Burgers vectors $\mathbf{b}_1$ and $\mathbf{b}_2$. (c) An alternative method for producing a twist grain boundary in smectic materials is to shear the two grains in opposite directions. This leads to two antiparallel screw dislocations both of magnitude $\mathbf{b}'_1$ and with a common line vector, t.

III. Low Angle Twist Boundary: Helicoid Section

To find an appropriate model for low angle twist boundaries in lamellar block copolymer systems, we begin with an aligned bicrystal that contains no boundary, Figure 3a. A hypothetical process to create a low angle twist boundary between these two grains involves slight rotation of one grain with respect to the other about an axis of rotation passing normal to the plane of the boundary and through the centers of the two grains, as in Figure 3b. This is the only correct way to produce a pure twist boundary in a material with a three dimensional lattice such as a metal. The resulting boundary consists of an array of two sets of mutually *orthogonal* screw dislocations[50] in the plane of the grain boundary with Burgers vectors $\mathbf{b}_1$ and $\mathbf{b}_2$. However, since our lamellar block copolymers only have one dimensional lattice symmetry, we can use a different hypothetical process to create a twist boundary, as shown in Figure 3c. Instead of rotating the two grains with respect to one another, consider shearing the two grains in opposite directions, while preserving lamellar thickness. This results in two *parallel* screw dislocations of the same magnitude but of opposite sign. These two dislocations share a common line of action, t. The displacement vectors, both denoted $\mathbf{b}'_1$, are no longer proper Burgers vectors but simply the total displacement of the lamellar planes at the edge of the grains. This sheared boundary would not be a pure twist boundary for a material with a three dimensional lattice. Also the shearing process would normally induce shear stresses in the grains on either side of the boundary and, thus, is not a generally permissible hypothetical route for the forma-

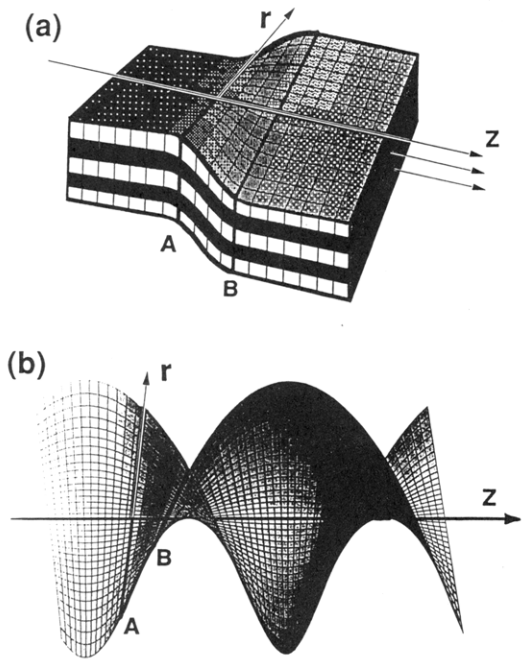

Figure 4. Helicoid section twist grain boundary morphology. (a) Lamellar material with a low angle twist grain boundary. The lamella undergo a slight "ripple" in this boundary region which is concentrated between positions A and B. (b) The IMDS in the grain boundary region is modeled with the boldly outlined section of the right helicoid minimal surface which is also delimited by A and B. The z-axis of the helicoid, as on the mathematical surface (b), is repeated for each helicoid section of the stack of IMDS's in (a). [Computer graphic of right helicoid by J. T. Hoffman of GANG.]

tion of twist boundaries. However, since the lamellar block copolymer has a smectic structure, the pure twist grain boundary and the boundary produced by this shearing process are indistinguishable.

The equivalence of twist and shear in this case can be appreciated as follows: Note in Figure 3b that the Burgers vector $\mathbf{b}_2$ lies within a lamellar plane where the material may be considered to be essentially a fluid, without periodic symmetry. Due to the lack of periodicity along $\mathbf{b}_2$ there is no reference frame available for the measurement of $\mathbf{b}_2$ and no way of observing this displacement. Thus for lamellar systems the pure twist process also leads to parallel, but opposite, screw dislocations with displacement vectors $\mathbf{b}'_1$. Alternatively, if we reconsider the shearing process, which is the other hypothetical process leading to this single array of parallel screw dislocations, we find that the previously mentioned problem with shear stresses in the free pseudocrystal on either side of the boundary is also meaningless for the smectic diblock structure. Due to the fluid nature of the structure within the lamellar planes, such a shear stress can relax without any alteration of the observable structure of the two grains. The set of two parallel screw dislocations illustrated in Figure 3c for lamellar diblocks is also used to quantify the lamellar grain boundaries in the A* phase.[44]

Having considered the general geometrical requirements for a twist boundary in a lamellar diblock material, we now turn to the modeling of the actual intermaterial dividing surface given these constraints. Although we have just shown that there is no difference between shear and twist in our system (at least for small angles), we will continue to use the term twist in our discussion rather than shear. At small amounts of twist the lamella can simply "ripple" slightly to undergo the required change of direction as shown in Figure 4a. This ripple can be modeled by a section of a classically known minimal surface, the helicoid. Figure 4b shows a portion of a helicoid. The boldly outlined section AB of the helicoid fits between two lamellar grains to achieve a small angle twist reorientation. The helicoid may be generated by moving a straight line, which is normal to the z-axis, along the z-axis at a constant rate and at the same time rotating this line about the z-axis at a constant rate. The relative rates of translation and rotation with respect to the z-axis determine the pitch of the helicoid. A higher pitch helicoid rotates through a greater angle for a given z-translation than a lower pitch helicoid. Mathematically, the helicoid remains minimal for any value of the pitch.[51] The helicoid sections used to model the grain boundaries are, however, only finite parts of the helicoid minimal surface which is infinite in extent. Mathematically, these finite sections are only approximately minimal. As can be appreciated from Figure 4a, the helicoid section boundary is actually made up of many stacked sections of helicoids, all of which rotate much less than a full turn about the z-axis. All these helicoids have z-axes that are perpendicular to the *plane*[52] of the grain boundary.

The IMDS† in the helicoid twist boundary can be visualized by starting with the bold line labeled A on the left grain of Figure 3b. This line represents the boundary between the planar lamellar interface in the unperturbed, left hand grain and the twisted IMDS† in the grain boundary region. Now move line A perpendicular to its length, directly across the region between the two grains, and rotate it at a constant rate so as to evenly distribute the twist necessary for it to move continuously into bold line B, of the right hand grain. By this process, line A has traced out a portion of a helicoid surface.

The equation of the helicoid section boundary is[53]

$$(x,y,z) = (r\cos\phi, r\sin\phi, s\phi) \qquad (1)$$

$$0 \le \phi \le \alpha \qquad 0 \le r \le D/2$$

$$s = 2\pi/\text{pitch} = \text{function}\ (D, \text{molecular parameters})$$

Here α is the twist angle of the boundary. The parameter r is the radius of the helicoid: the distance from the helicoid axis (z-axis) to any point on the surface. The maximum value of r is limited to the half-width of the grain, $D/2$, where D is the grain size. The parameter s determines the relationship between the rate of rotation of the generating line (line A in Figure 3b) and the rate of its translation along the z-axis: pitch $= 2\pi/s$. The value of the parameter s can be experimentally determined from TEM micrographs.

Figure 5 shows a TEM tilt series of a low angle ($\sim 10°$) twist boundary in SB 80/80. The tilt of 20° between Figure 5a and 5b is about an axis approximately parallel to the helicoid axis of the grain boundary region, as indicated on the micrographs. In order to understand the grain boundary geometry in these micrographs, we utilize ray tracing simulation. Figure 6 shows schematically how the inclination of a set of flat lamella (no grain boundary) with respect to the projection direction changes both the observed lamellar spacing and the contrast. The projected image that is observed is a function of the lamellar long period, L, the section thickness, h, and the angle of inclination of the lamella in the sample with respect to the projection direction. Contrast is maximized and lamellar spacing is minimized in a projection directly along the lamellar planes. As the lamellar planes become increasingly inclined with respect to the projection direction, the contrast undergoes damped oscillations while the observed lamellar spacing increases. The projected lamellar spacing is given by, $\mathcal{L} = L/\cos\gamma$, where γ is the angle of lamellar inclination defined in the figure. Contrast disappears

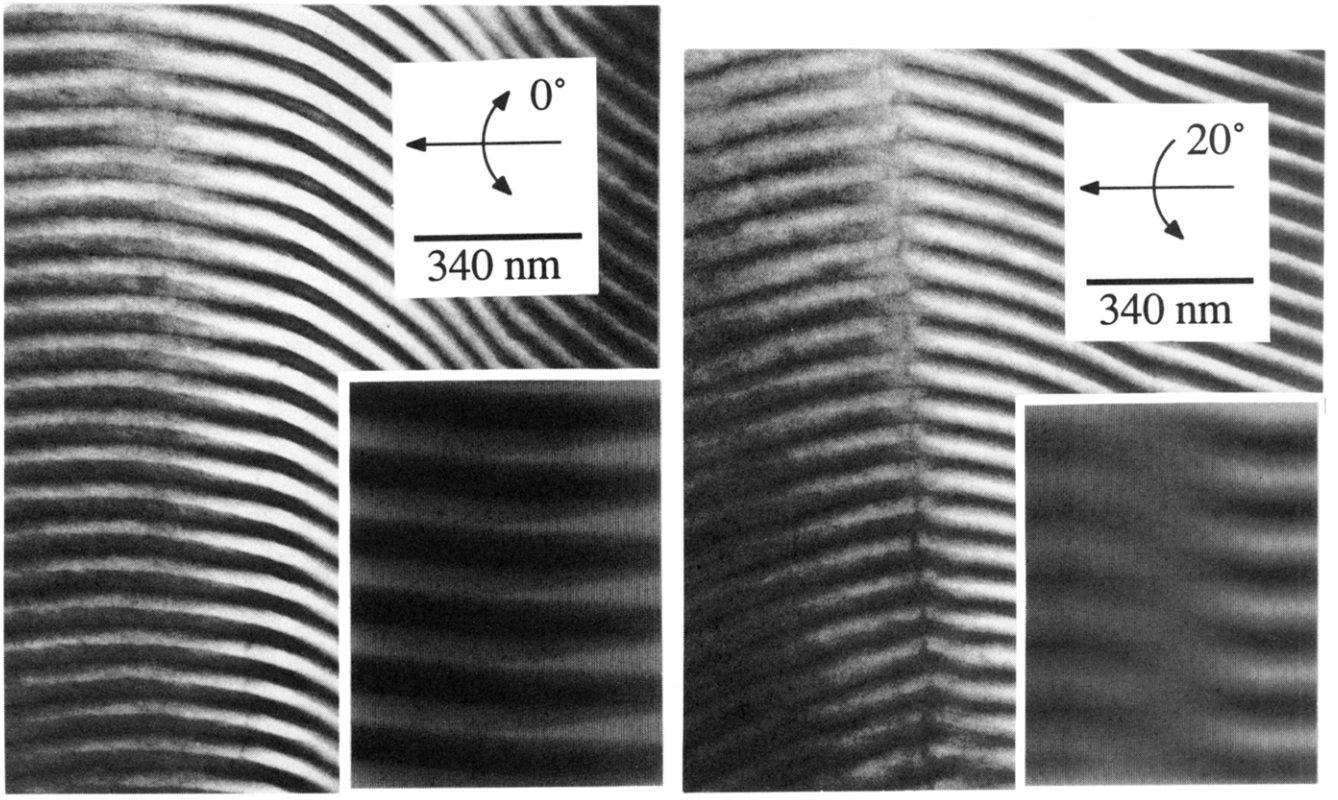

Figure 5. TEM tilt series of a helicoid section twist grain boundary (~10°) in SB 80/80. (a) The boundary and corresponding ray tracing computer simulation (inset) are viewed from a 0° tilt projection direction. (b) The specimen in the microscope and the corresponding computer simulation have been tilted by 20° about the axis shown. This tilting produces similar changes in the images of the specimen and the simulation.

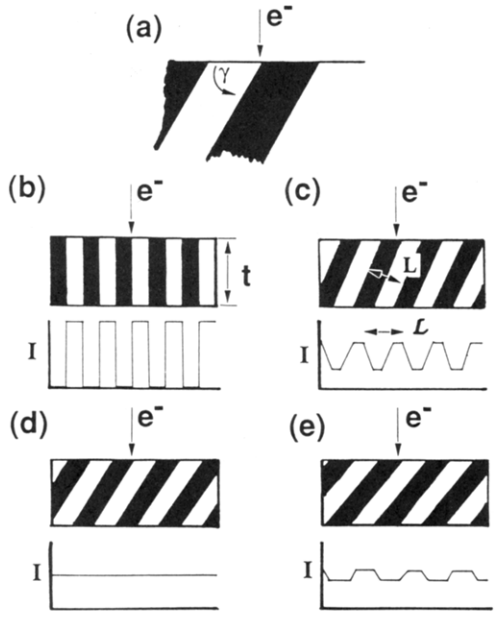

Figure 6. Illustration of the variation of bright field TEM projections of lamellar structures in samples of thickness h, as a function of the amount that lamella are inclined with respect to the electron beam. (a) The inclination of the lamella is measured by the angle γ. (b–e) The observed repeat spacing of the projected structure becomes progressively larger as γ decreases. The true long period, L, and the observed repeat distance, $\mathcal{L}$, are marked in (c). The electron intensity in the projected images is denoted by **I**. The contrast, or variation in **I**, undergoes damped oscillations as γ decreases. Contrast decreases from a maximum in (b) to zero in (d) but then reappears with further decrease in γ in (e).

periodically when $\gamma = \sin^{-1}(nL/2h)$, where n is an even integer. Angles where contrast is a local maximum of the damped oscillation are given by this same expression with n an odd integer. In Figure 6 changes in lamellar contrast are produced by changing the inclination of the lamella in the sample, while maintaining the projection direction of the electrons normal to the sample film. In the microscope the sample may also be tilted such that the electrons project in a direction that is no longer normal to the sample film; this also produces changes in lamellar spacing and contrast. In this case, it is possible to produce observed lamellar spacings that are less than the true long period.

Figure 7 shows ray tracing computer simulations of two tilt series for a 10° low angle twist boundary with the postulated helicoid IMDS†. In Figure 7a the tilt is about the z-axis of the helicoid whereas in Figure 7b the tilt axis is about an axis both normal to the z-direction and approximately normal to the lamellar planes. In Figure 7a, simulation C corresponds to projecting directly down the radial direction of the helicoid at a position halfway along the z-axis extent of the helicoid section. In this projection, the continuous nature of both the light and dark lamella through the grain boundary region is apparent. When the projection direction is tilted by ±10° about the z-axis (Figure 7a simulations B and D), lamellar contrast is enhanced on one side of the boundary and disappears almost completely on the other side of the boundary. This is because, for the 10° twist boundary, this 10° tilt aligns the projection direction perfectly with the lamella on one side of the boundary. On the other side of the boundary the lamellar orientation corresponds to the first contrast minimum discussed in the previous paragraph. In this case each ray encounters the same amount of both lamellar phases. Further tilting to ±20° (Figure 7a simulations A and E) leads to the restoration of moderate contrast for lamella on both sides of the boundary. Now, however, it appears that the twist boundary is of a discontinuous nature; the light and dark lamella do not match up across the boundary. We know

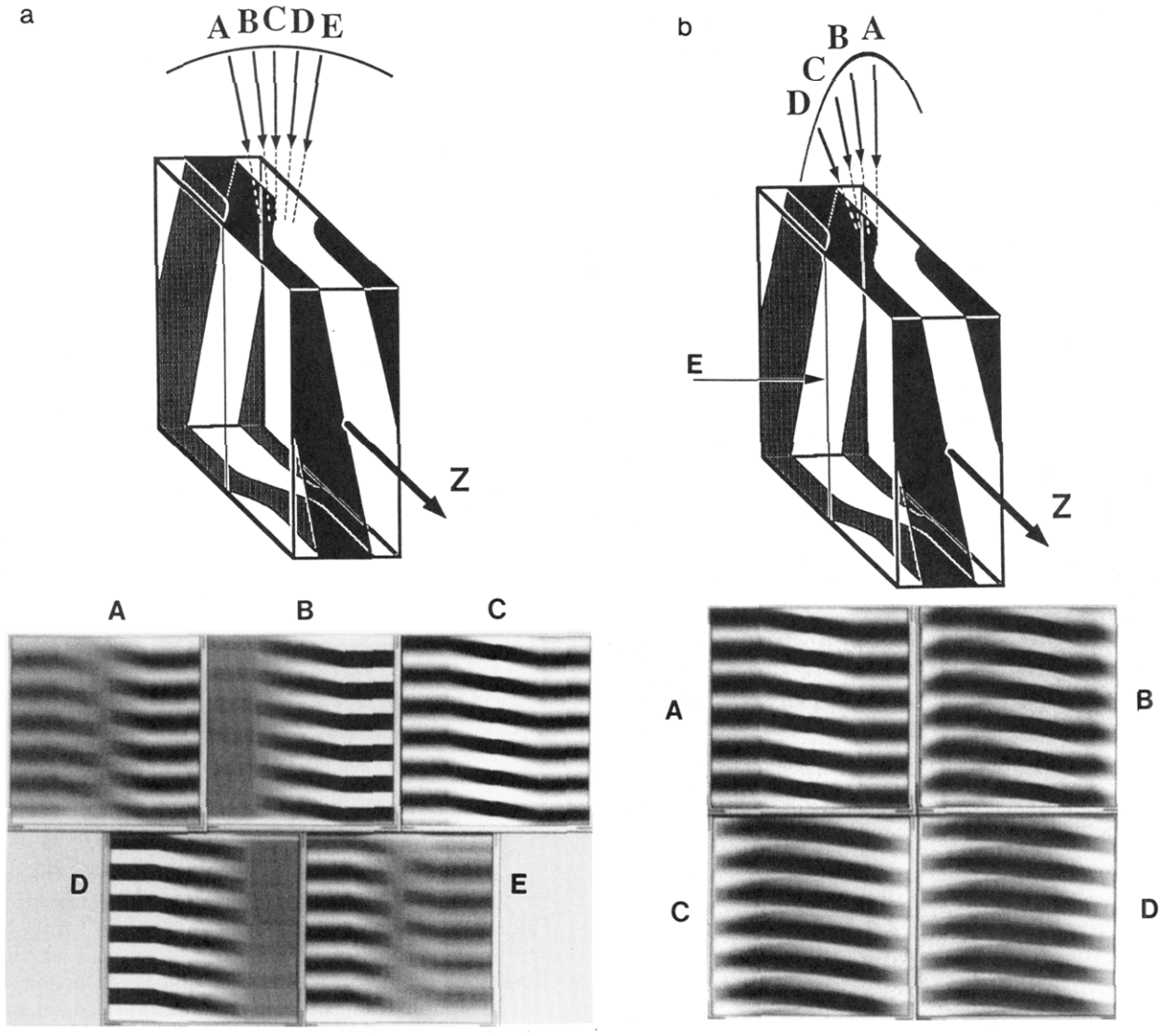

Figure 7. Computer ray tracing simulations of a tilt series on 10° helicoid section twist grain boundaries. (a) Tilt about the *z*-axis of the helicoid. The central projection of the series, C, is along the radial direction of the helicoid section. Projections B and D correspond to tilting from position C by ±10°, and projections A and E correspond to tilting for position C by ±20°. (b) Tilting about the axis labeled E produces projections A, B, C, and D for tilts of 0, 15, 30, and 45°, respectively. Projection along the E direction produces no image contrast.

this to be an artifact of projection. If the image in Figure 5b were examined on its own without the benefit of a TEM tilt series and the set of simulations in Figure 7a, an observer might draw the incorrect conclusion that this type of grain boundary involves a break in lamellar continuity.

In Figure 7b, simulation A is the same as Figure 7a simulation C. Now we tilt back about an axis parallel to direction E by 15, 30, and 45° to produce simulations B, C, and D in Figure 7b which are characterized by the development of interleaved light and dark wedgelike regions in the image of the grain boundary. Projection along direction E produces no image contrast. Thus it is apparent that the only helicoid sections that are observable by TEM are those that happen to be situated nearly edge-on to the electron beam direction.

Comparison of the TEM tilt series in Figure 5 and the simulations in Figure 7 show that in the experimental image in Figure 5a the projection is through the helicoid section boundary in the same orientation as simulation C or D in Figure 7b. Compare the interleaved dark and light wedgelike regions in the micrograph with the inset C simulation in Figure 7b. The polymer sample was then tilted in the TEM by 20° about the axis shown in the micrograph to produce the experimental image in Figure 5b. This tilt is of the same direction and magnitude as that between Figure 7a simulations C and A. However, this tilt about the *z*-axis is occurring with an approximately 30° back-tilt about axis E, corresponding to C in Figure 7b. Comparison of the micrograph in Figure 5b with an inset of simulation A in Figure 7a shows that, regardless of the 30° back-shift, the 20° side-to-side tilt has transformed both the TEM image and the simulation from what appears in projection to be continuous lamella to what appears to be a discontinuous grain boundary. The fact that not only the grain boundary in the sample and the simulation look the same in projection but also the simulated and experimental images vary in the same way with tilt is compelling evidence for the helicoid model of low angle twist boundary morphology.

Note also that since we are observing thin sections, we only have information about the extent of a grain in the plane of this section and no information about the grain size normal to the plane of the section. It is evident from eq 1 that in order to fully specify the helicoid section grain boundary geometry we must know the grain size, D, in the radial direction, r, as defined in Figure 4. Because we can only observe helicoids that have their radial directions nearly normal to the plane of the TEM specimen, there is no way of actually measuring the grain size in the radial

direction. Further note that we do not observe whole helicoid section boundaries but only a small part that is contained between two parallel microtomed planes which are essentially normal to the helicoid radial direction. It is reasonable to assume that the average grain size in the direction normal to the microtoming planes is the same as that observed in the plane of the specimen (i.e. equiaxed grains) by micrographs such as Figure 1. Methods for rigorous measurements of grain size from two dimensional sections are available using quantitative stereology.[54] However, in our diblocks the presence of gentle lamellar distortions and disclinations as well as grain boundaries leads to enough ambiguity in delineating the exact boundaries of some grains that these rigorous methods are impractical. However, we can make the observation that most grains observed in all three molecular weight diblocks fall in the size range from 2 to 5 μm. No correlation was observed between grain size and molecular weight. However, it is known that grain size increases somewhat with slower solution casting and with thermal annealing.

Due to the use of trigonometric functions in the mathematical expression for the helicoid section, eq 1, and in the equation for the other twist boundary morphology presented below, it is convenient to express lengths in dimensionless "mathematical units". Mathematical units, abbreviated "mu", are defined such that one long period of the lamellar structure is equal to 2π mu. Thus mu's are larger for higher molecular weight diblocks. Lamellar long periods, L, for the three diblocks used in this study were determined by small angle X-ray scattering (SAXS) in order to obtain the following relationships between physical and mathematical length units for each polymer: L (20/20) = 38.7 nm = 2π $mu_{20/20}$; L (40/40) = 62.5 nm = 2π $mu_{40/40}$; L (80/80) = 106 nm = 2π $mu_{80/80}$. These SAXS results compare well with previous long period measurements for these three diblocks.[55]

Experimental grain boundary widths, W, for helicoid section twist boundaries where measured from TEM micrographs for all three molecular weights. Helicoid section boundaries with twist angles less than about 5° where not observed, most likely because they do not cause enough distortion of the lamellar structure to be imaged by TEM. Helicoid section boundaries with twists larger than about 15° were also not observed. The absence of higher angle helicoid section boundaries will be addressed in GB-III using grain boundary energy calculations. Many helicoid section grain boundaries were observed in the twist range from about 8 to 12°, although the measurement of the twist angle from TEM micrographs involves an uncertainty of about ±2°. Grain boundary widths were measured for helicoid section boundaries with twists of 10 ± 2°, for grain sizes, D, of approximately 2–5 μm. There is also considerable uncertainty in measuring W from micrographs. We report the range of W for SB 20/20, 40/40, and 80/80 measured in nm and also normalized by the long periods of the corresponding diblocks. In order to obtain these W ranges we measured 42 boundaries in SB 20/20, 29 boundaries in SB 40/40, and 32 boundaries in SB 80/80. From these widths we then calculate the s values under the assumption of a 10° twist. For SB 20/20, 40/40, and 80/80 the ranges of helicoid boundary widths were 120–150, 190–250, and 320–420 nm, respectively. For all three molecular weights, W/L was in the approximate range 3–4, resulting in a range of s values from 110 to 140 mu/rad. Thus, when measured in dimensionless units that scale with the size of the lamellar structure, the helicoid section boundary width is independent of molecular weight. Figure 8 compares approximately 10° helicoid twist grain boundaries in SB 20/20 and 80/80. Both micrographs are at the same magnification. Aside from the generally larger size of the 80/80 morphology, notice that both boundaries are approximately $3L$ in width.

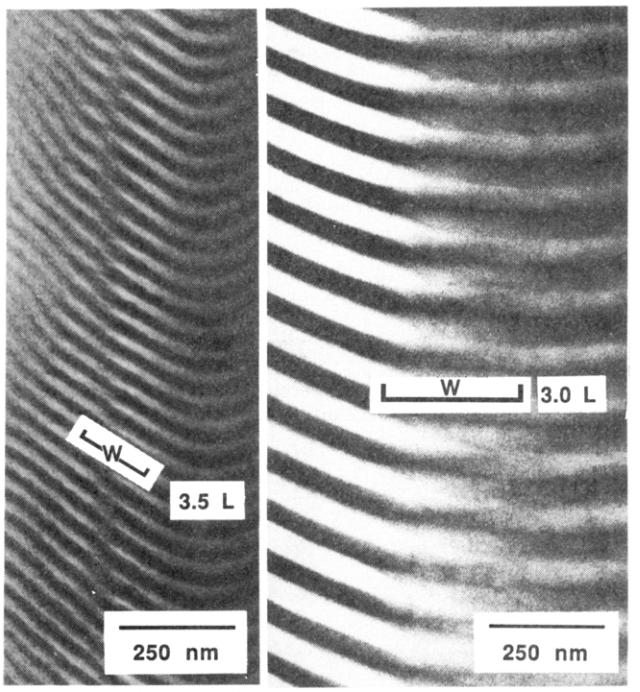

Figure 8. Comparison of 10° helicoid section twist boundary widths in (a) SB 20/20 and (b) SB 80/80. The micrographs are at the same magnification. The projection in both cases is along a direction about midway between Figure 7a projections C and B. This is a 5° tilt about the z-axis from the C direction. The boundary width, W, is measured using the corresponding long period, L. Both boundaries are approximately $3L$ in width.

The helicoid section boundary is not the only possible solution for smoothly joining two sets of lamella separated by a twist misalignment. The helicoid section might be replaced by some array of more closely spaced screw dislocations. The dislocations of such an array would then act on a local scale in order to achieve the same total reorientation of the lamella. Kléman[42] has predicted that such an array would consist of mutually orthogonal dislocations. In the following sections it will be shown how such a set of orthogonal dislocations may occur even though the smectic structure has only one dimensional symmetry. Kléman additionally predicted that the interface associated with such an array of the screw dislocations would be a periodic minimal surface; however, he did not elaborate further. In the following section we provide direct experimental evidence of such a periodic area minimizing twist boundary morphology.

IV. Scherk's First Surface Twist Boundaries

Scherk's first surface (also known as Scherk's doubly periodic surface) has been proposed as a model for a 90° twist boundary in lamellar systems.[22,26] In this case the grain boundary IMDS† approximates a minimal surface discovered in the 1830s by H. Scherk.[56] This surface is found by smoothly joining two sets of evenly spaced planes that meet orthogonally. Scherk's first surface, is shown in three dimensional perspective in Figure 9. Axes x and y lie in the plane of the grain boundary, and z is normal to it. The portion of the surface where the two sets of lamellae come into contact consists of a doubley periodic array of saddle regions. Each saddle is crossed by a pair of orthogonal screw dislocations (Figure 14a).

Thomas *et al.*[22] have published a TEM micrograph of such a 90° twist boundary in a SB diblock copolymer

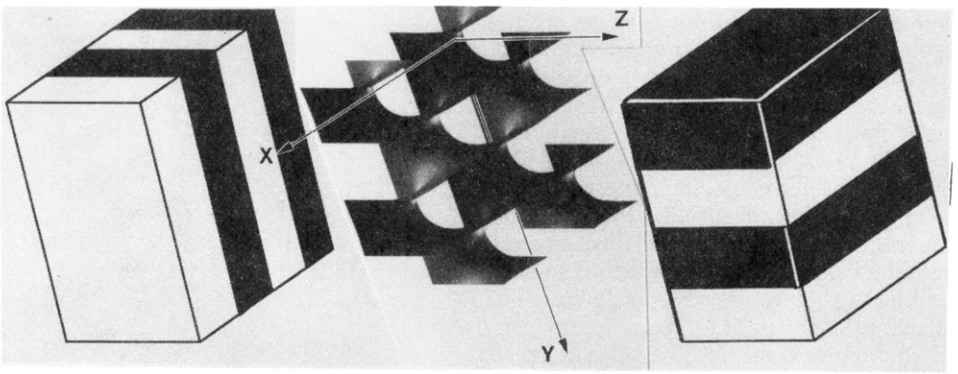

Figure 9. Three dimensional perspective view of Scherk's first surface shown between two diblock copolymer grains twisted 90° with respect to one another. [Computer graphic by J. T. Hoffman of GANG.]

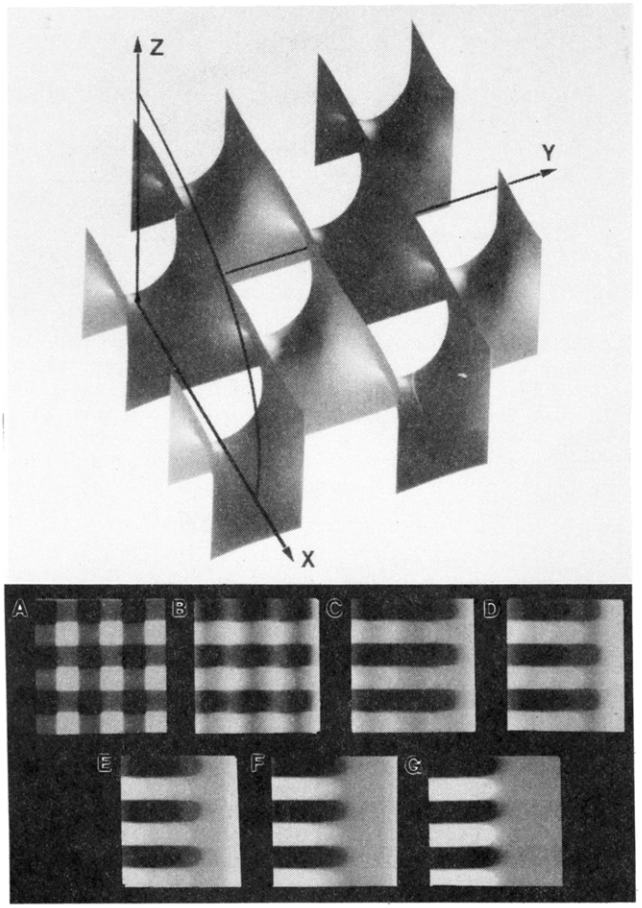

Figure 10. Computer ray tracing simulation of a TEM tilt series on a 90° twist Scherk surface grain boundary. Simulation A corresponds to projecting directly down the z-axis of the Scherk surface, while simulation G corresponds to projecting down the x-axis. Simulations B through F correspond to projection direction spanning the 90° tilt angle between A and G in 15-deg increments. [Scherk surface perspective computer graphic by J. T. Hoffman of GANG.]

solution cast thin film (~1000 Å), along with a computer ray tracing projection of Scherk's first surface. This interfacial geometry allows microphase continuity across the grain boundary and minimizes unfavorable contact between unlike microphases. Figure 10 depicts a simulated tilt series starting with a projection down the z-axis, simulation A, and tilting in the xz-plane in 15-deg increments until simulation G which projects in the x-direction. Simulation G corresponds to the micrograph and simulation previously given by Thomas *et al.*[22]

In the thin film case substrate/surface energy considerations lead to lamella that either lie in the plane of the substrate or perpendicular to the substrate. This resulted in only twist boundary angles of 90°, separating regions of the two different lamellar orientation, to be observed in this special system. Since lamellar twist grain boundaries in bulk cast films (1 mm or more thick) occur at angles other than 90°, we now extend the model based on Scherk's first surface to general twist angles.

Three different Scherk grain boundaries were found in SB 20/20 and 80/80 samples, all of which had twist angles of approximately 80°, but which varied greatly in the orientation within the thin sample sections. This presented an opportunity to compare TEM tilt series covering very different ranges of projected geometry for similarly shaped boundaries. The goniometer stage on the TEM offers a limited tilt range so that all projection geometries are not accessible with a single sample. As with the helicoid grain boundaries, ray tracing simulations were also performed for the Scherk morphology.

Figure 11a shows a TEM micrograph of a Scherk twist boundary in SB 20/20. The projection zone axis is the z-axis of the Scherk surface. This Scherk boundary has a twist of about 80°. Figure 11b shows a computer ray tracing simulation of a z-axis projection of a 80° Scherk interface. The z-axis projection shows the true twist angle, but generally, projecting an image of an arbitrarily oriented grain boundary into two dimensions obscures the true geometry.

Figure 12 gives a tilt series of another ~80° Scherk grain boundary, this time in SB 80/80. The boundary actually has a significant *tilt* component ($\theta \approx 60°$). Here we have used a normal typeface "tilt" to mean the orientation of the sample with respect to the incident electron beam in the TEM and an italicized "*tilt*" to refer to the geometrical degree of freedom for grain boundaries illustrated in Figure 2a. The sample is progressively tilted around an axis in the plane of the boundary so that the grain boundary comes into view showing the saddle regions in perspective. The boundary region of Figure 12a is seen edge-on in projection so that it appears as a narrow line-like feature in the image. A corresponding ray tracing simulation is shown as an inset on each micrograph in Figure 12. In Figure 12b the specimen has been tilted in the microscope by 25° abount the axis indicated. This causes the foreshortened projection of the boundary plane to come into view. In this image we see rows of bumps which result from the projection of the Scherk surface array of saddle IMDS†'s into the plane of the image. Further tilting to 50° about the same axis produces the micrograph in Figure 12c in which more of the grain boundary plane comes into view.

Figure 13 shows the third ~80° Scherk twist boundary, also in SB 80/80, with the corresponding inset computer simulation. While in Figure 12 the Scherk saddle regions are visible as bumps along the light PS lamella in the grain boundary region, the other set of saddles which must be present along the PB lamella are difficult to see. If the

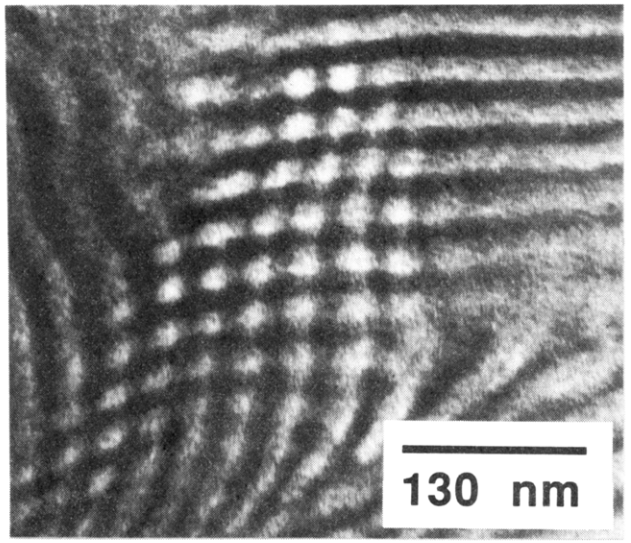

(a)

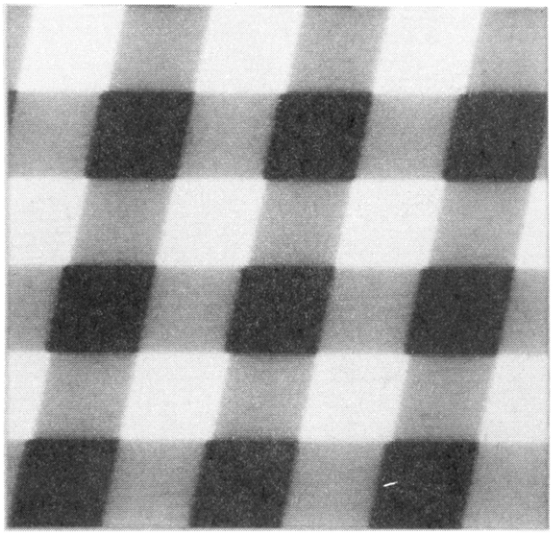

(b)

Figure 11. 80° Scherk twist boundary in SB 20/20. (a) TEM micrograph with a z-axis projection direction. (b) Corresponding ray tracing simulation. Three levels of intensity are present both in the TEM image and in the simulation. Black regions result from the matching of PB lamella across the boundary. White regions result from the matching of PS lamella across the boundary, and gray regions result when PS and PB lamella come into contact and are separated by a Scherk saddle IMDS.

Scherk surface grain boundary model is valid, then Figure 9 and the ray tracing simulations indicate that we should see saddles in both the light and dark lamella in the grain boundary region. The saddles are gray and thus should appear as dark bumps in the light lamella and as light bumps in the dark lamella. As is apparent in Figure 9, the saddles in adjacent rows of the Scherk surface array should be staggered like squares of the same color on a checker board. In Figure 13 saddle bumps are clearly visible in both the light and dark lamellar rows in the grain boundary region. Careful examination reveals that these saddles are staggered between adjacent dark and light rows.

Scherk himself presented a relatively simple analytical representation for a whole family of minimal surfaces, smoothy joining two sets of parallel, equidistant planes meeting at any twist angle.[56] All Scherk surfaces, regardless of twist angle, are minimal surfaces. To visualize a twisted Scherk surface one simply needs to imagine rotating the lamella from the 90° orientation shown in Figure 9. The saddle regions distort appropriately to maintain zero mean curvature of the IMDS† and the connectivity of the two separate microphases across the boundary.

The general twist, Scherk minimal surface is given by

$$(x, y, z) = \left(u, v, \frac{1}{\sin \alpha} \ln \left\{\frac{\cos u}{\cos[u \cos \alpha + v \sin \alpha]}\right\}\right)$$

Where α is the twist angle defined in Figure 2.

Figure 14 shows how Scherk surfaces, viewed along the z-direction (normal to the plane of the grain boundary), and the Burgers vectors $\mathbf{b}_1$ and $\mathbf{b}_2$ change as the twist angle is varied. In contrast to the low angle helicoid twist boundary, where only one displacement vector was possible due to the lack of translational periodicity along a direction in the lamella, in the high angle twist boundary the crosshatched moiré pattern produced by the meeting of the misoriented lamellar planes creates a two dimensional symmetry net in the plane of the boundary, and thus two vectors are required to describe the twist defect. Unlike the case of the helicoid, these two vectors are proper Burgers vectors. One set of the screw dislocations in this boundary is right-handed, as indicated by **b** parallel to **t**, where **t** is the line vector of the dislocation. The second set of dislocations, perpendicular to the first, consists of left-handed screws for which **b** is antiparallel to **t**.

At 90° twist, when viewed normal to its plane, the Scherk surface resembles a checkerboard where each shaded square indicates the up (lighter shading) and down (darker shading) curvature of a single saddle region separating the two types of material where unlike lamellar planes cross each other. The unshaded squares corresponded to a matching of lamellar layers of like materials across the grain boundary. The letters S or B beside beside each row indicate the material, polystyrene (S) or polybutadiene (B), that is on the top side of each saddle in the row when viewed from the arbitrarily chosen side of the boundary used in Figure 14a. Also, in each row the regions of matching lamella correspond to the matching of the type of microphase, S or B, designated for that row. It must be emphasized that this figure shows the interfacial surface only. When the volumes separated by this interface are filled with light (PS) and dark (PB) materials and a ray tracing projection is carried out along the z-direction, the result is a cross bar pattern, as shown in Figure 10 simulation A and in the TEM of Figure 11. The white and black regions in the simulation and micrograph correspond to regions of lamellar plane matching indicated by the unshaded squares in Figure 14a. The white results from matching of PS planes, while the black results from matching of PB planes. The gray regions in the simulation and the micrograph occur when projecting down through saddle regions (shadded in Figure 14a) so that roughly half of the material through which electrons pass is PB and half is PS (assuming that the boundary plane is in the middle of the microtomed section).

This type of crossed hatched grain boundary symmetry with alternating regions of crystal matching and mismatching is general for twist boundaries, as is illustrated in texts on defects in atomic crystals.[39] Note that the Burgers vectors, $\mathbf{b}_1$ and $\mathbf{b}_2$, each traverse two saddle regions instead of just one. This is because the unit cell on the periodic net of saddles (bold outlines in Figure 14a,b) contains two saddles one with PB above the IMDS† and the other with PS above. Thus a displacement of two saddle diagonals is required to bring the surface into coincidence with itself.

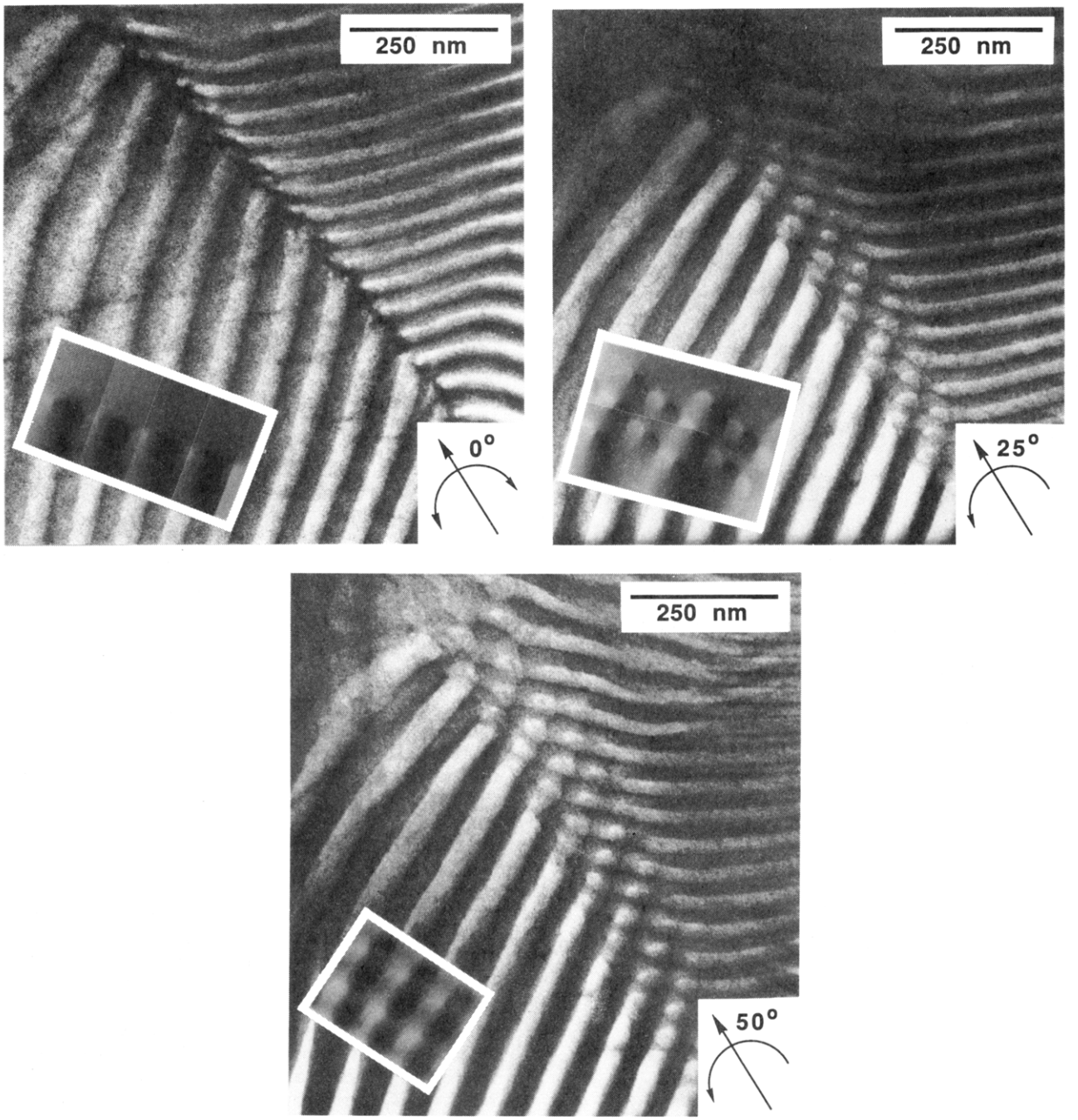

Figure 12. TEM tilt series of an 80° Scherk surface twist grain boundary in SB 80/80. (a, top left) 0° tilt projection from which the plane of the grain boundary is viewed edge on. The inset is ray tracing simulation. (b, top right) The 25° tilt projection brings a foreshortened projection of the grain boundary plane into view, revealing an array of Scherk saddles. The inset is ray tracing simulation. (c, bottom) The 50° tilt projection brings more of the grain boundary plane into view. The inset is ray tracing simulation.

Again referring to Figure 14, we see that as the twist angle decreases, each square saddle region distorts into a rhombus. This distortion of the saddles must occur with preservation of lamellar thickness, causing the saddle regions to become very elongated in the direction of the major diagonal at low twist angles. As the twist angle decreases, the Burgers vectors remain orthogonal, one increasing in magnitude ($\mathbf{b}_1$ along the major diagonal) while the other is decreasing ($\mathbf{b}_2$ along the minor diagonal). The increase of $\mathbf{b}_1$ occurs more rapidly, as the twist angle is decreased, than the corresponding decrease of $\mathbf{b}_2$. From dislocation theory we expect that the energy of each dislocation is proportional to $\mathbf{b}^2$; thus the 90° twist boundary should represent an energy minimum for Scherk surface interfaces, with the energy increasing as the twist angle is decreased. As 0° twist is approached, the saddle regions are actually drawn out to infinity along the major diagonal. The smaller Burgers vector approaches a minimum value for the Scherk surface, equal to the lamellar long period, while the larger Burgers vector diverges to infinity. Thus the energy of a single saddle region of interface also diverges as zero twist is approached. We show in GB-II, however, that this increase in energy with decreasing twist is a result of the extensive nature of this measure of grain boundary energy. As twist decreases, the size of the saddles increases. This leads to an increase in total energy. When measured on a per unit volume or per chain basis, however, the energy of the material in the grain boundary region will be shown to decrease with decreasing twist.

Figure 15 shows a TEM z-axis projection of a lower angle Scherk twist boundary in SB 40/40 which has an IMDS[†] similar to that illustrated in Figure 14b. Actually, the twist angle changes within this boundary. In the center

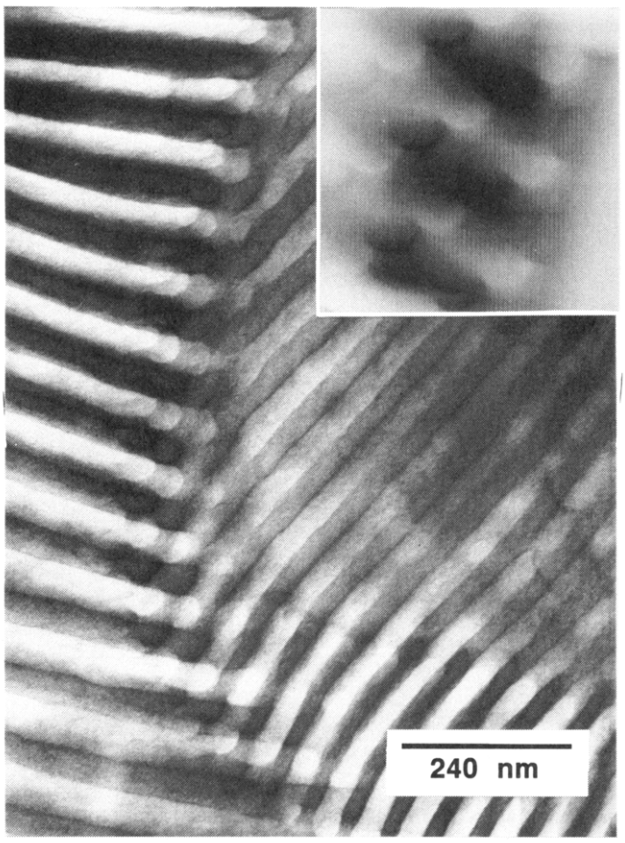

Figure 13. TEM micrograph of an 80° Scherk surface twist grain boundary in SB 80/80 clearly revealing a staggered array of saddle surfaces. The inset is ray tracing simulation.

of the micrograph the twist is about 30°, but in the lower right hand corner the twist changes to about 45°. The gray saddle regions and the white and black regions of PS and PB plane matching are clearly visible. They are drawn out into the rhombus shapes expected from the Scherk model at lower twist angles.

V. Very Low Angle Scherk Surfaces: Transition to the Single-Helicoid Screw Dislocation

The process of saddle elongation as the twist angle of the Scherk surface is decreased has been mathematically proven[57] to lead, in the limit of zero twist, to the production of a single helicoid. An observer located anywhere on the dislocation line $\mathbf{t}_2$ (Figure 14b) would see, as the twist of the Scherk surface approaches zero, the row of saddles that contains this line elongates to infinity in the direction of $\mathbf{t}_1$. This causes the saddles to eventually acquire the exact shape of a single helicoid. The dislocation line $\mathbf{t}_2$ becomes the z-axis of a helicoid which completes one full turn over what were previously the two saddle regions of a Scherk unit cell. As twist approaches zero, other rows of saddles along the adjacent dislocation lines, parallel to the $\mathbf{t}_2$ that we have chosen, will appear to the observer to move off to infinity and thus vanish. The resulting single helicoid is the core structure of a single screw dislocation, the only dislocation remaining from the orthogonal array of dislocations present in higher angle Scherk surfaces. This single screw dislocation is particularly interesting because, unlike screw dislocations in single phase atomic crystals, its core structure does not involve a structural singularity.

Figure 16a illustrates the structure that results when a Scherk grain boundary in a diblock is twisted to zero degrees. In this figure only the interfaces are shown, the light and dark phases are not filled in so that the core of the dislocation structure is visible. The letters S and B

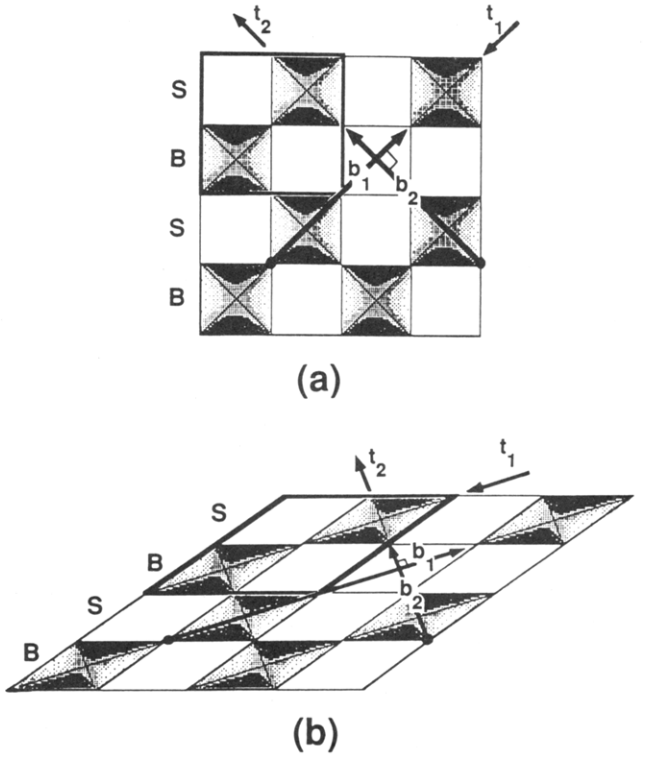

Figure 14. Scherk surface IMDS viewed from the z-axis direction for (a) 90° twist and (b) 45° twist. The open spaces correspond to holes in the Scherk surface where adjacent lamella of like material match up across the grain boundary. The designation S or B beside each row of the structure indicates where PS or PB lamella match up across the holes of the particular row. The shaded sections are the saddle surfaces, with dark shading indicating downward curvature and light shading indicating upward curvature. The Burger's vectors, $\mathbf{b}_1$ and $\mathbf{b}_2$, and line vectors, $\mathbf{t}_1$ and $\mathbf{t}_2$, of two orthogonal sets of screw dislocations are shown on the surfaces.

beside the figure indicate whether PS or PB is between the adjacent set of interfaces. Proceeding in the direction of the positive z-axis in Figure 16a, we find that two distinct types of IMDS†'s are encountered: PS-to-PB and PB-to-PS. The core structure of the screw dislocation, shown in Figure 16b, is a helicoid. This surface provides a nonsingular IMDS† in the core region. The single helicoid contains both types of interfaces, PS-to-PB and PB-to-PS. It is an orientable surface (a surface with two distinct sides), and the arrows in the figure indicate its PS-to-PB direction. Notice that on any one of the ruling lines (perpendicular to the z-axis) that make up the surface, the orientation of the surface (direction of the arrows in the figure) changes from one side of the z-axis to the other. Thus a ruling line sweeps out the helicoid surface, one side generates the PS-to-PB interface (this side is boldly outlined in the figure) and the other side generates the PB-to-PS interface. Notice in Figure 16a,b that the helicoid structure is actually doubly helical like the structure of DNA. Kléman has theoretically predicted that a right helicoid is the minimum energy configuration for a single screw dislocation in a smectic A liquid crystal.[42] The doubly helical illustration in Figure 16a is adapted from discussions of dislocations in smectic A layers by Bouligand.[58,59]

The key feature that distinguishes the single screw dislocation from the grain boundary morphologies discussed in this paper is that its projected image is invariant as the projection direction is rotated around the z-axis of the helicoid as long as the projection direction remains perpendicular to the z-axis. Figure 17 shows such a TEM tilt series of a 0° Scherk surface/single screw dislocation

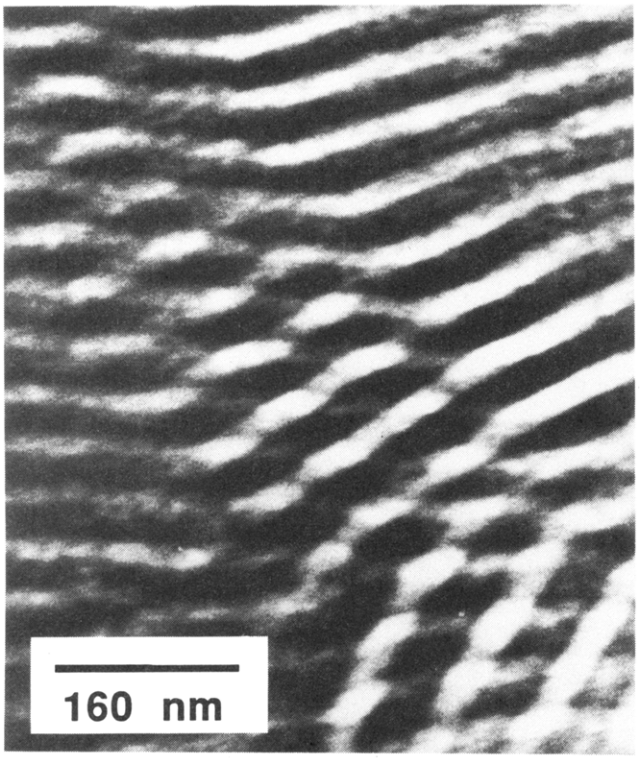

Figure 15. TEM micrograph of a z-axis projection of a Scherk boundary in SB 40/40. In the center of the micrograph the twist is about 30°, while in the lower right hand corner the twist changes to about 45°.

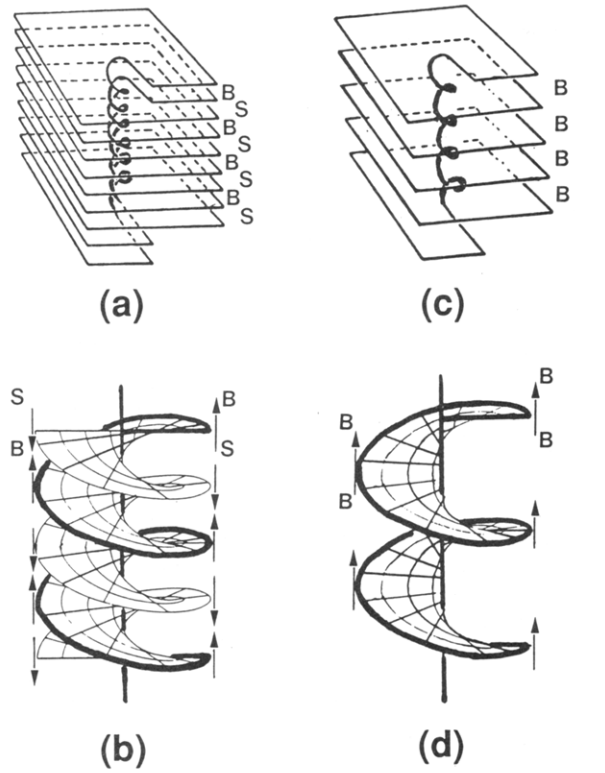

Figure 16. Single screw dislocation structure. (a) Single screw dislocation structure in a biphasic material [adapted from ref 58]. The letters S and B beside the layers indicate the alternating layers of PS and PB. (b) Right helicoid core structure of a single screw dislocation in a biphasic material. This is also the structure of the 0° twist limit of the Scherk surface. The arrows indicate the PS → PB direction of the IMDS. (c) Single screw dislocation in a single phase material. (d) The half-helicoid core structure of a single screw dislocation containing a structural singularity along the screw axis. No singularity is present in the biphasic material structure (a and b).

in a SB diblock copolymer system. In this case the material is actually a blend of 60 volume % SB 80/80, 20 volume % PS homopolymer (molecular weight 17 000), and 20 volume % PB homopolymer (molecular weight 21 000). One can see the delicate outline of the upward spiraling helicoid in the projected images. It is evident from the figures that the TEM image of the screw dislocation remains essentially the same as the projection direction is tilted over a range of 50° about the axis of the dislocation. The figure also shows a ray tracing simulation of a single helicoid screw dislocation as it would appear from any of the projection directions used in the TEM series. The agreement between the simulation and the micrographs is very convincing. The single screw dislocation, low angle Scherk surface appears very similar to some projections of the helicoid section boundary such as Figure 7a simulations A and E. However, the low angle Scherk surface may always be distinguished from the helicoid section since the projected image of the low angle Scherk is tilt invariant.

As shown in Figure 16c a screw dislocation in a crystal[50] can be described by analogy to the spiraling layers of a multilevel parking garage where a driver can move up or down by driving around the center of the garage. Figure 16d shows the surface which represents distorted crystal planes in the core structure for this type of screw dislocation. This screw surface is half a helicoid produced by rotating only the half of a generating line on one side of the z-axis. As indicated by the arrows in this figure, the screw surface cannot divide space into two separate volumes like the helicoid does. Importantly, the screw surface core structure has a singularity along the z-axis which is not present in the helicoid. In a single phase atomic crystalline solid there is only one type of material so the screw dislocation structure need not separate space. This would also be the case for a simple short rod smectogen in which the two ends of the rods are indistinguishable. Such a smectic material would be expected to have the screw dislocation structure shown in Figure 16c,d. However, as soon as the smectic rods have two distinct ends, that separate from one another, the helicoid or double helix screw dislocation is required in order to keep these two ends separated. Common smectics such as microemulsions and the diblock copolymers studied here, are analogous to rods with distinct ends and thus form the helicoid screw dislocation. The nonsingular core structure of the helicoid IMDS†, as discussed in GB-II, provides a relatively low energy morphology for the screw dislocation. The helicoid screw dislocation, which is the zero twist limit of the doubly periodic Scherk grain boundary, is analogous to a parking garage in which there are two sets of upward spiraling levels (S and B in Figure 16a) that always remain separated.

The helicoid that remains when the Scherk surface is twisted to zero is fundamentally different from the previously described helicoid section boundary. This difference is made apparent by comparing Figure 4a, which shows a helicoid section boundary, to Figure 16a,b. The helicoid section boundary is made up of many stacked sections of helicoids, all of which rotate much less than a full turn about the z-axis as one passes from one grain into the next. All these helicoids have z-axes that are perpendicular to the plane of the grain boundary. The helicoid that results when the Scherk surface is rotated to zero twist, however, has its z-axis in the plane of the grain boundary and it goes through many complete turns, one per lamella long period. This helicoid is the result of a single screw dislocation which remains in the sample even though the twist has been removed.

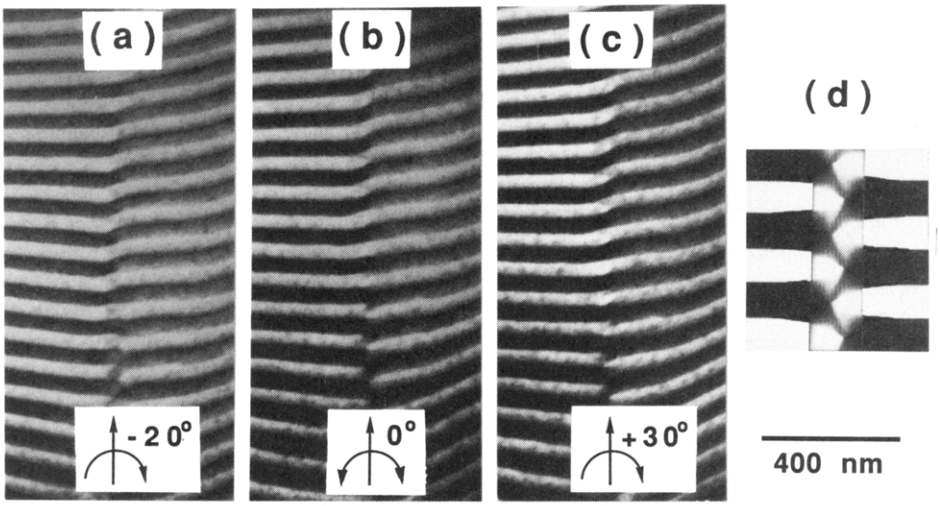

Figure 17. TEM tilt series of a 0° twist Scherk surface or single screw dislocation in a blend of 60 vol % SB 80/80, 20 vol % homopolystyrene (17 000), and 20 vol % homopolybutadiene (21 000). (a–c) TEM tilt series spanning 50° of a projection angle in a plane normal to the screw axis. The projected image of the dislocation core is invariant with tilt in this series. In all three projections one can see the spiraling levels of the single helicoid IMDS†. (d) Computer ray tracing simulation of a 0° twist Scherk surface projecting normal to the *z*-axis. These simulation conditions match all projections in the TEM tilt series.

On the other hand, the helicoid section boundary is two parallel but opposite screw dislocations that share a common line of action (Figures 3 and 4). One of these dislocations moves lamellar planes down while on the other side of the shared line vector the other dislocation moves the planes back up by the same amount. On driving around the center of a parking garage based on the helicoid section boundary, one would go down on one side and them back up on the other to complete a circuit while remaining on the same level. In fact, one could never change levels! The helicoid section boundary might thus be referred to as an "Escher parking garage" due to its similarity to the never ending staircase walked by the monks in M. C. Escher's print *Ascending and Decending*.

This parking garage analogy illustrates a fundamental topological difference between a bicrystal containing a helicoid section boundary and a bicrystal containing a Scherk boundary. It is apparent from Figure 9 that a Scherk boundary provides passageways that connect a lamellar layer of one microphase (PS or PB) to many other layers of the same material on the opposite side of the boundary. In the limit when the Scherk boundary is twisted to zero degrees, these tunnels become two nested spiraling ramps, each of which still allows access from one layer of microphase A (B) to any other layer of the same microphase. By contrast, the helicoid section provides no passages between lamellar layers. It is this topological difference that underlies the presence of only the parallel dislocations for the helicoid section while the Scherk surface contains the orthogonal pattern of two sets of screw dislocations commonly associated with twist boundaries in crystals. This topological difference may also be important for physical properties such as gas permeability and mechanical stiffness.[60]

When the helicoid section model is applied to a reasonably large grain ($D \geq 1$ μm), then beyond a few degrees in twist the lamellar planes also form a cross hatched moiré pattern when viewed in a projection normal to the grain boundary, along the *z*-axis in Figure 4a. However, in the helicoid case the planes which appear in projection to meet in a crossed pattern are actually at different levels in the sample, indicated by positions marked A and B in Figure 4a. They do not actually form a cross hatched pattern, but rather twist around without any interaction between different layers. Thus there is no single plane in which a two dimensional symmetry net can be constructed, and thus a second Burgers vector cannot be defined.

VI. Conclusions

In this paper we have presented TEM micrographs demonstrating structural models for localized twist boundaries in SB diblock copolymers. The intermaterial dividing surfaces in the grain boundary regions, and in other defect structures, have been designated IMDS† to distinguish them from the interfacial surfaces in equilibrium microdomain morphologies which are designated IMDS. The geometry of these interfaces was demonstrated by comparing experimental TEM images with ray tracing computer simulations of the model surfaces as the projection direction was systematically varied in both the experimental and simulated images. The two morphologies observed were found to have intermaterial dividing surfaces that approximate either Scherk's first (doubly periodic) surface or a section of a helicoid. The helicoid section boundary was observed at low twist angles, less than or equal to about 15°. The Scherk surface family of boundary morphologies, which consists of a doubly periodic array of saddle surfaces, was found over the entire twist range from 0 to 90°. As the twist angle approaches zero degrees, the Scherk surface grain boundary morphology is transformed into a single screw dislocation that has an intermaterial dividing surface with the geometry of a single helicoid. Direct TEM imaging of the detailed core structure of this screw dislocation was presented. These images demonstrate that in the lamellar diblock copolymer the screw dislocation core is nonsingular.

Acknowledgment. We wish to thank Dr. L. J. Fetters of Exxon for synthesizing the diblock copolymers and Profs. H. Karcher, R. Kusner, and P. Smith for discussions on differential geometry. Computer graphics of minimal surfaces were generated at GANG (the Center for Geometry, Analysis, Numerics, and Graphics) at the University of Massachusetts, Amherst, with the help of J. T. Hoffman. S.P.G. wishes to thank the organizers of the 1991 NSF Summer Research Institute on Graphics and Computation in Differential Geometry at which many difficulties in this research were resolved. Dr. G. Y. Kim prepared the diblock homopolymer blend sample in which the single helicoid screw dislocation morphology was discovered. J.G. acknowledges financial support in the

form of an AFOSR fellowship. J.G. would also like to thank Philip R. Thompson of MIT whose XImager (XIM) software package was used for displaying the simulations presented in this paper. Funding was provided by NSF-DMR 8907433, AFOSR 910078, CMSE 9022933, and DOE DE-FG02-86ER25015.

References and Notes

(1) Kinning, D. J.; Thomas, E. L.; Ottino, J. M. *Macromolecules* **1987**, *20*, 1129.
(2) Alward, D. B.; Kinning, D. J.; Thomas, E. L.; Fetters, L. J. *Macromolecules* **1986**, *19*, 215.
(3) Gido, S. P.; Thomas, E. L. Submitted for publication to *Macromolecules*.
(4) Gido, S. P.; Thomas, E. L. Manuscript in preparation.
(5) Gido, S. P.; Thomas, E. L. Manuscript in preparation.
(6) Helfand, E.; Wasserman, Z. R. *Macromolecules* **1978**, *11*, 960.
(7) Helfand, E.; Wasserman, Z. R. *Macromolecules* **1980**, *13*, 994.
(8) Ohta, T.; Kawasaki, K. *Macromolecules* **1986**, *19*, 2621.
(9) Hashimoto, T.; Fujimura, M.; Kawai, H. *Macromolecules* **1980**, *13*, 1660.
(10) Hashimoto, H.; Fujimura, M.; Hashimoto, T.; Kawai, H. *Macromolecules* **1981**, *14*, 844.
(11) Leibler, L. *Macromolecules* **1980**, *13*, 1602.
(12) Hasegawa, H.; Tanaka, H.; Yamasaki, K.; Hashimoto, T. *Macromolecules* **1987**, *20*, 1651.
(13) Fredrickson, G. H.; Binder, K. *J. Chem. Phys.* **1989**, *91*, 7265.
(14) Fredrickson, G. H.; Helfand, E. *J. Chem. Phys.* **1987**, *87*, 697.
(15) Gobran, D. Ph.D. Thesis, University of Massachusetts, 1990.
(16) Bates, F. S.; Fredrickson, G. H. In *Annual Review of Physical Chemistry*; Strauss, H. L., Babcock, G. T., Moore, C. B., Eds.; Annual Reviews Inc.: Palo Alto, CA, 1990; Vol. 41, p 525.
(17) Helfand, E.; Tagami, Y. *J. Chem. Phys.* **1972**, *56*, 3592.
(18) Helfand, E. *J. Chem. Phys.* **1975**, *62*, 999.
(19) Helfand, E.; Sapse, A. M. *J. Chem. Phys.* **1975**, *62*, 1327.
(20) Helfand, E. *J. Chem. Phys.* **1975**, *63*, 2192.
(21) Helfand, E.; Wasserman, Z. R. *Macromolecules* **1976**, *9*, 879.
(22) Thomas, E. L.; Anderson, D. M.; Henkee, C. S.; Hoffman, D. *Nature* **1988**, *334*, 598.
(23) Hashimoto, T.; Shibayama, M.; Kawai, H. *Macromolecules* **1980**, *13*, 1237.
(24) Bates, F. S.; Berney, C. V.; Cohen, R. E. *Macromolecules* **1983**, *16*, 1101.
(25) Anderson, D. M.; Thomas, E. L. *Macromolecules* **1988**, *21*, 3221.
(26) Thomas, E. L.; Gido, S. P. In *Materials Research Society Symposium Proceedings*; Buckley, A., Gallagher-Daggitt, G., Karasz, F. E., Ulrich, D. R., Eds.; Materials Research Society: Pittsburgh, PA, 1990; Vol. 175; p 315.
(27) Schwarz, H. A. *Gesammelte Mathematische Abhandlungen*; Springer: Berlin, 1890; Vols. 1 & 2.
(28) Hyde, S. T.; Andersson, S. *Z. Kristallogr.* **1984**, *168*, 1.
(29) Hyde, S. T.; Andersson, S.; Ericsson, B.; Larsson, K. *Z. Kristallogr.* **1984**, *168*, 213.
(30) Hyde, S. T.; Andersson, S.; Larsson, K. *Z. Kristallogr.* **1986**, *174*, 237.
(31) Andersson, S.; Hyde, S. T.; von Schnering, J. G. *Z. Kristallogor.* **1984**, *168*, 1.
(32) Andersson, S.; Hyde, S. T.; Larsson, K.; Lindin, S. *Chem. Rev.* **1988**, 221.
(33) Scriven, L. E. *Nature* **1976**, *263*, 125.
(34) Fredrickson, G. H. *Macromolecules* **1991**, *24*, 3456.
(35) Olvera de la Cruz, M.; Mayes, A. M.; Swift, B. W. *Macromolecules* **1992**, *25*, 944.
(36) Richards, R. W.; Thomason, J. L. *Macromolecules* **1983**, *16*, 982.
(37) Csernica, J.; Baddour, R. F.; Cohen, R. E. *Macromolecules* **1989**, *22*, 1493.
(38) Verhoeven, J. D. *Fundamentals of Physical Metallurgy*; John Wiley and Sons: New York, 1975.
(39) Hirth, J. P.; Lothe, J. *Theory of Dislocations*, 2nd ed.; John Wiley and Sons: New York, 1982.
(40) Smith, C. S. *Metall. Rev.* **1964**, *9*, 1.
(41) de Gennes, P. G. *The Physics of Liquid Crystals*; Oxford University Press: New York, 1974.
(42) Kléman, M. *Points, Lines, and Walls*; John Wiley and Sons: New York, 1983.
(43) Goodby, J. W.; Waugh, M. A.; Stein, S. M.; Chin, E.; Pindak, R.; Patel, J. S. *Nature* **1989**, *337*, 449.
(44) Renn, S. R.; Lubensky, T. C. *Phys. Rev. A* **1988**, *38*, 2132.
(45) Srajer, G.; Pindak, R.; Waugh, M. A.; Goodby, J. W.; Patel, J. S. *Phys. Rev. Lett.* **1990**, *64*, 1545.
(46) Ihn, K. J.; Pindak, R.; Zasadzinski, J. A. N. *50th Annual Meeting of the Electron Microscopy Society of America (EMSA)*; San Francisco Press: Boston, 1992; p 278.
(47) Ihn, K. J.; Zasadzinski, J. A. N.; Pindak, R.; Slaney, A. J.; Goodby, J. *Science* **1992**, *258*, 275.
(48) Kinning, D. J.; Thomas, E. L.; Fetters, L. J. *J. Chem. Phys.* **1989**, *90*, 5806.
(49) Anderson, D. M.; Bellare, J.; Hoffman, J. T.; Hoffman, D.; Gunther, J.; Thomas, E. L. *J. Colloid Interfacial Sci.* **1992**, *148*, 398.
(50) Read, W. T., Jr. *Dislocations in Crystals*; McGraw-Hill: New York, 1953.
(51) A ruled surface is a surface which is swept out by a family of straight lines. The only ruled minimal surfaces are the plane and the helicoid. Two helicoids of different pitches differ by a multiplicative scaling factor. We can understand why the helicoid remains minimal for any pitch as follows: The curvature of a plane curve changes by a factor of $1/\delta$ when the curve itself is scaled by a factor δ. This implies that the mean curvature scales by the same multiplicative factor. Thus the mean curvature of an $H = 0$ surface such as the helicoid is scale invariant.
(52) The *plane* of the grain boundary is a hypothetical, mathematical plane that separates the two grains and is located at the center of the physical grain boundary region. It does not correspond to the IMDS†. In the helicoid section grain boundary the plane of the boundary is normal to the z-axis. In the Scherk surface boundary, the plane of the boundary is the xy-plane.
(53) Struik, D. J. *Lectures on Classical Differential Geometry*, 2nd ed.; Dover: New York, 1961; pp 61, 62.
(54) Underwood, E. E. *Quantitative Stereology*; Addison-Wesley: Reading, MA, 1970.
(55) Kinning, D. J. Ph.D. Thesis, University of Massachusetts, 1986.
(56) Scherk, H. F. *J. Reine Angew. Math.* **1835**, *13*, 185.
(57) Hoffman, D.; Wolgemuth, M. Manuscript in preparation.
(58) Bouligand, Y. *J. Phys.* **1972**, *33*, 525.
(59) Bouligand, Y. In *Dislocations in Solids*; Nabarro, F. R. N., Ed.; North Holland: Amsterdam, 1980; pp 300–347.
(60) Gido, S. P. Ph.D. Thesis, Chemical Engineering, Massachusetts Institute of Technology, 1993; Chapter 8.